ELSEVIER

Comput. Methods Appl. Mech. Engrg. 191 (2002) 5899–5922

Computer methods in applied mechanics and engineering

www.elsevier.com/locate/cma

SUPG stabilized finite element resolution of the Navier–Stokes equations Applications to water treatment engineering

P. Vellando [a,*], J. Puertas [b], I. Colominas [a]

[a] *Group of Numerical Methods in Engineering (GNME), Dpto. de Métodos Matemáticos y de Representación, ETS de Ingenieros de Caminos, Canales y Puertos, Universidad de La Coruña, Campus de Elviña, 15071 La Coruña, Spain*

[b] *Area de Ingeniería Hidráulica, Dpto. de Métodos Matemáticos y de Representación, ETS de Ingenieros de Caminos, Canales y Puertos, Universidad de La Coruña, Campus de Elviña, 15071 La Coruña, Spain*

Received 5 June 2002; received in revised form 8 August 2002

Abstract

In this paper an analysis of the viscous incompressible flow has been carried out, from the very definition of the governing equations, up to the resolution of some practical problems, passing through the comprehensive study of the stabilized finite element techniques used in their resolution. As a consequence of this analysis, a code based upon a realistic interpretation of the forces has been written, which allows for the modelling of the open channel flow, with optimum results in the resolution of some benchmark and real flow problems related with the wastewater industry.

Keywords: Viscous incompressible flow; FEM; Navier–Stokes; SUPG; Wastewater treatment

1. Introduction

The finite element method was first developed in the fifties by Turner et al. so as to solve some structural problems of the aeronautical industry [42]. The application of the finite element method to the resolution of the flow problems requires some modifications with respect to the formulation used for the structural stress analysis problems that were its first application. Some of these modifications have been borrowed from the finite difference or finite volume approaches, and many others have been specifically developed for finite elements. In the early seventies we find many works regarding not only the mere existence and consistency of the solution to these flow problems [3,6,29] but also many works that give a finite element solution to the Navier–Stokes equations [31,39,47]. Since then, the finite element method is a powerful tool for the

* Corresponding author. Tel.: +34-981-167000; fax: +34-981-167170.
E-mail address: vellando@iccp.udc.es (P. Vellando).
URL: http://caminos.udc.es/gmni.

0045-7825/02/$ - see front matter
PII: S0045-7825(02)00503-0

resolution of the Navier–Stokes equations, which will be used in this work to solve the viscous incompressible flow.

The material we are going to deal with when solving the flow problems, is of a fluid nature, and therefore it has not a fixed shape, which is instead a function of time. In addition to Newton's second law, that rules any dynamic problem, an equation that ensures for the conservation of mass should be verified. Moreover, the Navier–Stokes equations are a set of differential equations with respect to space and time in which both the pressure and the velocity are the unknowns. As a consequence, the finite element formulation used for the conventional structural analysis cannot be applied straightforwardly.

When applying the finite element analysis to the problems of the rigid body, the weighted residual method can be exclusively applied to Newton's second law, which for statics clearly turns out to be the equilibrium equation. On the contrary, when dealing with fluids, the shape is not any more conserved, and apart from stating the equilibrium of momentum, we have to ensure for the continuity of mass. Consequently, we have two equations to be verified at the same time, and the finite element formulation should also account for the verification of both. The only set of unknowns in the conventional structural analysis is that of the displacements; as a consequence, the system obtained thanks to the application of the finite element method gives the displacements in the structure depending on the stiffness matrix (that features the structure), and the load vector. In the flow problems, we are headed towards the so-called mixed finite element method, in which both the velocity and the pressure set of unknowns have to be treated simultaneously.

Depending on how these two sets of equations and unknowns are tackled, several different approaches have been developed. Some authors [9,26] agree to classify the different approaches to solve the viscous incompressible flow by the finite element method into three different categories: these are the mixed (or velocity–pressure integrated), the penalty and the segregated methods. The mixed method is the most intuitive of these approaches, and is based upon carrying out a similar analysis for the continuity equation to that used for the momentum equation, keeping both velocity and pressure as the unknowns up to the end of the problem. This apparently straightforward way of dealing with our equations is not as simple as it appears to be, and it may be the reason of the obtaining of a meaningless solution when used in connection with a faulty basic element as shown in the early works by some authors [39]. The so-called mixed formulation leads to some consistency problems in the obtaining of the solution when a wrong choice in the basic functions has been made. As a consequence, the penalty and segregated methods have been developed to overcome these difficulties. In this work, a 2D algorithm of each of those three different types will be developed, verified and used in the analysis of some practical problems and discussed.

The 2D Navier–Stokes equations assume a flow that takes place on a two-dimensional plane, and it is therefore laminar in that sense. A fully 3D resolution of the flow, apart from leading us to tough memory requirements, both in storing memory and in CPU time, would involve some problems in the modelling of the free water surface. The shallow water formulation has been considered as a way of including the third dimension in the model, being able to give a meaningful solution for flows in which the depth is small compared to the horizontal dimension. The integration in depth of the 3D Navier–Stokes formulation causes the dependence of the continuity equation with respect to depth, and consequently the appearance of some quasi-non-linear terms that depend on both the velocity and the depth. These equations are solved by means of a newly developed iterative algorithm, which will be solved on a mixed formulation basis to be described later in the text.

The use of a Galerkin formulation, that takes weighting functions equal to trial functions when solving the Navier–Stokes equations, may lead to some problems of instability in the solution of the flow problems by the finite element method. To avoid this difficulty, some so-called stabilization procedures have been released since the MAFELAP conference in 1975 [17,18,47]. The stiffness matrix resulting from conventional structural finite element analysis is symmetric, instead the 'stiffness' matrix obtained for fluids is non-symmetric and the use of symmetric weighting functions may lead to some instability problems. The faster

the flow turns, the more non-symmetric the coefficient matrix becomes. In practice, this is featured by the appearance of some spurious node-to-node oscillations also known as 'wiggles'. One way of avoiding these oscillations is to carry out a refinement in the mesh, such that convection no longer dominates on an element level, but this refinement turns to be a memory resources sink. This source of instability can be avoided by using a stabilization technique, being the streamline upwinding Petrov–Galerkin (SUPG) [21] and Galerkin least squares (GLS) [23] the most commonly used of these methods.

A stabilization technique of the SUPG type will be used for all the algorithms considered in this work. These technique, first developed by Hughes and Brooks [7,21,22], succeeds in eliminating the spurious velocity field oscilations, without carrying out a severe refinement in the mesh, by considering weighting functions that differ from trial functions in an upwinding term. This method was first released for the transport equation, and its generalization to the Navier–Stokes equations brings an additional problem; that is the appearance of an excessive diffusion normal to the flow. The SUPG method eliminates this spurious crosswind diffusion by considering an artificial diffusion that acts only in the direction of the flow. All the particulars regarded in this introduction and some others will be further considered in the following chapters.

2. Governing equations

The dynamic and the continuity equations make up the so-called Navier–Stokes equations, that govern the viscous incompressible flow. These equations are named after their discoverer, the French civil engineer Claude-Louis Navier (1785–1836), who in 1821 formulated the equations that rule the incompressible flow. The Navier–Stokes equations also bear the name of the Irish mathematician George Gabriel Stokes (1819–1903), who not knowing the previous discoveries made by Navier, Poisson and Saint-Venant, re-obtained the Navier–Stokes equations for slightly different assumptions, and published these works in 1845.

Using the indicial we can express the Navier–Stokes equations as

$$u_{i,t} + u_j u_{i,j} = -\frac{1}{\rho} p_{,i} + \nu u_{i,jj} + f_i \qquad u_{i,i} = 0 \text{ in } \Omega \tag{1}$$

together with the boundary and initial conditions

$$\begin{aligned} &u_i]_{\Gamma_1} = b_i \qquad \sigma_{ij} n_j]_{\Gamma_2} = t_i, \\ &u_i(x_j, 0) = u_{i0}(x_j), \end{aligned} \tag{2}$$

where u_i is the velocity, p is the pressure, f_i is the body force per unit mass, ρ is density, ν is the cinematic viscosity, Γ_1 and Γ_2 are two non-overlapping subsets of the piecewise smooth domain boundary Γ, b_i is the velocity vector prescribed in Γ_1, t_i is the traction vector prescribed on Γ_2, σ_{ij} is the stress along the boundary Γ_2, and n_j is the outward unit vector normal to Γ_2.

The 2D Navier–Stokes equations will be used in this work to solve some benchmark problems with very good results, as will become clear later in the text. The 2D or laminar (in the sense of planar) Navier–Stokes equations do not take into account the third dimension in space, and provide with the velocities and pressures of a theoretical planar flow. Nevertheless, for many real flow problems, the third dimension in space is very important and the 3D Navier–Stokes equations should be considered. The three-dimensional Navier–Stokes equations result in a very large-dimensioned system of equations that involves tough computational requirements. Moreover, the 3D schemes present a great difficulty in the treatment of the free surface. For flows in which the horizontal dimension is small compared to depth, the shallow water formulation can be successfully employed as a simplification of the 3D Navier–Stokes equations [45]. This simplification can be used when the main direction of the flow is the horizontal one and the distribution of the horizontal velocity along the vertical direction can be assumed as uniform. The shallow water equations

assume that the vertical acceleration of the fluid is negligible and that a hydrostatic distribution of the pressure can be adopted. When the 2D Navier–Stokes equations are used, no attention is paid to the third dimension in space, and the continuity equation is only held on a 2D basis. So as to get the adequate information about the variations in depth along the flow, either a 3D Navier–Stokes equation or the shallow water equations should be used.

The shallow water equations are used in this work to solve same problems in which the flow can be assumed as shallow. Integrating in depth the 3D Navier–Stokes equations the shallow water equations are obtained as

$$\begin{aligned} &h_{,t} + hu_{i,i} + u_i h_{,i} = 0, \\ &u_{i,t} + u_j u_{i,j} = -gh_{,i} + \nu u_{i,jj} + g(S_{0i} - S_{fi}), \end{aligned} \tag{3}$$

where h is the depth, g is the gravity force and S_{0i} and S_{fi} are the geometric and friction slopes. Let us make some comments on the evaluation of the friction slope.

All the flows found in civil engineering practice can be featured by the Reynolds number (UL/ν, where U and L are the characteristic velocity and length of the flow and ν is the kinematic viscosity that depends on the fluid nature). For small Reynolds numbers, the flow can be regarded as laminar, and the streamlines are parallel to each other. As the Reynolds number is increased, a chaotic, random and intrinsically unsteady type of motion appears. If these turbulent effects are to be solved by using the Navier–Stokes equations, a very refined mesh would be required to capture the eddies taking place on a wide range of length scales, and a special attention should be devoted to the unsteady resolution of the turbulent phenomena, that take place at a very high frequency [44]. The mesh refinement and the time step required for this purpose are not yet computationally affordable. Consequently, a turbulence model should be implemented in order to evaluate these turbulent eddies. Most of these turbulence models are based upon decomposing the involved variables into a mean value (within a time increment) and a fluctuating term that depends on time. As a consequence of this approach, a term that evaluates the turbulent losses as a function of a so-called 'eddy viscosity' ν_t, is obtained. To evaluate this eddy or turbulent viscosity, a specific turbulence model such as the k–ε model should be introduced. Making use of these turbulence models, the turbulent viscosity is calculated for each time step and position, allowing for the capturing of these eddies [16,24,28,38].

The turbulent effects can also be evaluated on an overall basis. The evaluation of the friction slope on a Manning basis [43] permits to evaluate empirically the overall energy losses taking place in the fluid flow, including those related with the turbulent effects. This formulation does not capture the turbulent eddies taking place within the fluid flow but takes into account the overall turbulent energy losses, moreover keeps the full Navier–Stokes formulation, being ready to incorporate a two-equations turbulence model. By doing so, the frictional slope can be evaluated as

$$S_{fi} = \frac{n^2 u_i \sqrt{u_j^2}}{R_h^{4/3}}, \tag{4}$$

where R_h is the hydraulic radius and n is the Manning coefficient.

The use of this formulation allows for a realistic interpretation of the forces taking place within the flow and provides a meaningful tool for the resolution of some practical flows as will be seen in the examples.

3. Finite element formulation

3.1. Mixed laminar formulation

This formulation is directly obtained from the application of the weighted residuals method on both the dynamic and continuity equations. In the Galerkin method, the test functions are taken equal to the trial

functions, in terms of which the unknowns are interpolated. We are going to introduce a SUPG stabilization of the algorithm by considering an additive term $\bar{p}_i$ in the weighting functions. Applying the weighted residuals method in this way on both the dynamic and continuity Navier–Stokes equations, it is obtained

$$\begin{aligned}
&\int_{\Omega_h} w_i^h (u_{i,t}^h + u_j^h u_{i,j}^h - f_i^h)\,\mathrm{d}\Omega + \nu \int_{\Omega_h} w_{i,j}^h u_{i,j}^h\,\mathrm{d}\Omega - \frac{1}{\rho}\int_{\Omega_h} w_{i,i}^h p\,\mathrm{d}\Omega \\
&\quad - \int_{\Gamma_2} t_i^h w_i^h\,\mathrm{d}\Gamma_2 + \sum_e \int_{\Omega_e} \bar{p}_i^h \left(u_{i,t}^h + u_j^h u_{i,j}^h - \nu u_{i,jj}^h + \frac{1}{\rho} p_{,i}^h - f_i^h\right)\mathrm{d}\Omega = 0; \qquad (5)\\
&\int_{\Omega_h} q^h u_{i,i}^h\,\mathrm{d}\Omega = 0,
\end{aligned}$$

where $\overline{w}_i = w_i + \bar{p}_i$ are the SUPG weighting functions for the dynamic equation and q are the weighting functions for the continuity equation. The h superscript stands for the discretization being carried out in our formulation, which will be made in terms of a Q1P0 basic element.

This formulation should verify in addition to the governing equations, some consistency conditions, the most restrictive of which is the Ladyzhenskaya–Babuska–Brezzi (LBB), or divergence–stability condition [6]. A wrong election in this basic element may fail to verify this condition and prevent the whole algorithm from converging. The Q1P0 basic element, used in connection with the present formulation, even not being strictly divergence–stability stable, has shown to produce stable and efficient solutions.

Once the elementary matrices are evaluated and assembled, the integral equation (5) can be expressed in matrix notation as

$$\begin{aligned}
&\mathbf{M}_\upsilon \frac{\partial \underline{\upsilon}}{\partial t} + \mathbf{C}_\upsilon(\mathbf{u},\mathbf{v})\underline{\upsilon} + \nu \mathbf{A}_\upsilon \underline{\upsilon} - \mathbf{B}\mathbf{p} = \mathbf{f}, \qquad (6)\\
&\mathbf{B}^T \underline{\upsilon} = \mathbf{0},
\end{aligned}$$

where $\mathbf{M}_\upsilon$ is the mass matrix, $\mathbf{C}_\upsilon(\mathbf{u},\mathbf{v})$ is the convective matrix, $\mathbf{A}_\upsilon$ is the viscous matrix, $\mathbf{B}$ is the pressure matrix, $\mathbf{f}$ is the external forces vector, $\mathbf{p}$ is the pressure vector, $\mathbf{u}$ is the velocity vector in the x-direction, $\mathbf{v}$ is the velocity vector in the y-direction and $\underline{\upsilon}$ is the velocity vector [43].

For the derivatives with respect to time included in the first term of the first equation in (6), a finite difference backward differencing approach will be used in order to transform our partial differential system into an algebraic one.

The convective term $\mathbf{C}_\upsilon(\mathbf{u},\mathbf{v})\underline{\upsilon}$ that appears in (6), is not the product of a coefficient matrix times a vector of unknowns, but a non-linear velocity-dependent function. This term should be eliminated in order to transform the resulting system into a linear system of equations. The numerical scheme to be used for this transformation is going to be a so-called successive approximation method, that can be mathematically expressed as

$$\int_{\Omega_h} \overline{w}_i u_j u_{i,j}\,\mathrm{d}\Omega \approx \int_{\Omega_h} \overline{w}_i u_j^{n-1} u_{i,j}^n\,\mathrm{d}\Omega \qquad (7)$$

and has shown to provide with good results in the resolution of the Navier–Stokes equations [13]. This method converges linearly to the solution in opposition to some others, like the Newton–Raphson method, which do it in a quadratic way in the vicinity of the solution. Still, the necessity of an appropriate initial guess in the Newton–Raphson method may prevent the solutions from converging [25], and a continuation technique, is often required.

The mixed formulation so-implemented is still quite expensive in terms of storing memory requirements, with the associated coefficient matrix of the resulting system being $2M + N$ dimensional, where M and N are the number of the velocity and pressure unknowns respectively.

3.2. Penalty laminar formulation

The main difficulty found when obtaining a numerical solution for the Navier–Stokes equations is that apart from verifying the dynamic constitutive equation, the solutions must satisfy in addition the incompressibility condition. The mixed finite element formulation leads to a system in which both velocity and pressure are taken as unknowns. Nonetheless, besides the problems entailed in the election of the basic elements in order to allow for the divergence–stability condition to be held, mixed methods result in a large-dimensioned system of equations. Therefore, not only a larger dimension has to be handled with its corresponding increased memory requirements, but also the stiffness matrix is found to be radically different to the narrow-band type of matrix, which is preferred for the direct resolution of the systems of equations. To overcome these shortcomings, the penalty formulation was proposed by Zienkiewicz [46], based upon the variational calculus theory, and was soon extended and applied by many authors [7,19,20,40]. The penalty formulation provides with the possibility of imposing the incompressibility constraint without solving an auxiliary pressure equation, by replacing the continuity equation with the expression

$$u_{i,i} = -\varepsilon p, \tag{8}$$

where the so-called penalty parameter ε is a number close to zero. This equation is incorporated into the dynamic equation, and therefore a system that depends on both velocity and pressure is transformed into a velocity-dependant single equation, that converges to the fully incompressible problem as ε approaches zero. Once we have applied the weighted residuals method, the following integral dynamic equation is obtained:

$$\int_{\Omega_h} w_i^h (u_{i,t}^h + u_j^h u_{i,j}^h - f_i)\,\mathrm{d}\Omega + \nu \int_{\Omega_h} w_{i,j}^h u_{i,j}^h\,\mathrm{d}\Omega + \int_{\Omega_h} \frac{1}{\varepsilon} u_{i,i}^h w_{i,i}^h\,\mathrm{d}\Omega - \int_{\Gamma_2} t_i^h w_i^h\,\mathrm{d}\Gamma_2 + \sum_e \int_{\Omega_e} \bar{p}_i^h \left(u_{i,t}^h + u_j^h u_{i,j}^h - \nu u_{i,jj}^h - \frac{1}{\varepsilon}(u_{i,i}^h)_{,i} - f_i \right) \mathrm{d}\Omega = 0 \tag{9}$$

which is solved for pressure. Once the velocity field has been obtained, the pressure field can be calculated as a post-processing result, by using the formula

$$p^h = -\frac{1}{\varepsilon} u_{i,i}^h. \tag{10}$$

The solution to equation (9) will approximate that of the initial problem as ε tends to zero, provided that the penalty consistency condition is verified. If not, the use of the penalty formulation could lead to the obtaining of a non-singular coefficient matrix associated to the penalty term. As ε tends to zero, this term may dominate the system of equations, therefore the whole problem could be over-constrained, and the only possible solution could be the trivial one. When carrying out an exact integration of the penalty term, '*locking*' occurs and the only possible solution is the trivial one. The discrete formulation in (9) would not be consistent and the algorithm would not achieve convergence [20].

This problem can be avoided by making a so-called *selective reduced integration* of the elementary matrices involved in the resolution of the problem. A reduced numerical integration consists in using a quadrature rule that is not exact for the polynomials considered. The use of a one point Gauss quadrature rule for the integration of the quadratic functions in the penalty term, transforms the associated 'penalty' matrix into a rank deficient matrix and consequently '*unlocks*' the obtaining of a non-trivial solution. For more details on this topic you can refer to [8].

Once the elementary matrices are evaluated and assembled, the integral equation in (9) can be expressed in matrix notation as

$$\mathbf{M}_v \frac{\partial \underline{v}}{\partial t} + \mathbf{C}_v(\mathbf{u}, \mathbf{v})\underline{v} + \nu \mathbf{A}_v \underline{v} + \frac{1}{\varepsilon}\mathbf{B}_\varepsilon \underline{v} = \mathbf{f}, \tag{11}$$

where $\mathbf{M}_v$ is the mass matrix, $\mathbf{C}_v(\mathbf{u}, \mathbf{v})$ is the convective matrix, $\mathbf{A}_v$ is the viscous matrix, $\mathbf{B}_\varepsilon$ is the penalty matrix, $\mathbf{u}$ is the velocity vector in the x-direction, $\mathbf{v}$ is the velocity vector in the y-direction, $\mathbf{f}$ is external forces vector and $\underline{v}$ is the velocity vector. The non-linearities and the derivatives with respect to time are solved by using a successive approximation method and a backward differencing scheme, in the same way as we proceeded for the mixed formulation [43].

The penalty method succeeds in solving the Navier–Stokes equations with great memory savings due to the smaller number of equations to be solved, producing meaningful and stable solutions thanks to the use of the so-called reduced integration as seen in the previous section. Anyhow, the accurateness of the method depends on the election of the parameter ε. For very small values of ε, the weight of the penalty term in the stiffness matrix happens to cancel the amount of information contributed by the viscous term, which is very small in comparison. This information is consequently truncated and dropped from the equations. The penalty parameter should consequently be chosen depending on the word length of the computer. On the other hand, if the selected penalty parameter is too large, this choice may spoil the whole procedure, as ε is wanted to tend to zero so as to allow for convergence. Consequently, the choice of ε is not a trivial task, and a wrong selection in the parameter may lead to a meaningless solution. Moreover, the penalty formulation achieves a great reduction in the storing requirements, compared to the mixed formulation (the $2N + M$ equations in the mixed formulation are reduced to a $2N$ dimensioned system in the penalty formulation). Still, the stiffness matrix is far from being a narrow band type of matrix despite the renumbering of the nodes. Interesting and more recent SUPG penalty formulations can be found in [10,15,43].

3.3. Segregated laminar formulation

To overcome the drawbacks arising from the resolution of the integrated velocity–pressure and penalty formulations of the viscous flow, the so-called 'segregated methods' have been proposed in order to reduce the memory requirements when solving the Navier–Stokes equations. Some of the most commonly used of these segregated methods, that obtain the flow variables in a sequential way, are the fractional step method [11,33], and those based upon a SIMPLE algorithm [4,34,36] followed by [9,41,48] among others. An algorithm based upon the SIMPLE method is described in this section.

Many of these shortcomings are not present in the so-called segregated methods, which are broadly employed by many authors so as to solve the Navier–Stokes equations. Following the success of the finite volume method [32], several authors adopted the formulation in the SIMPLE and SIMPLEST methods to the finite element approach. These segregated finite element schemes give solution to the problem of the viscous incompressible flow, by employing a procedure in which the velocity and pressure unknowns are not obtained simultaneously but in a sequential way. The segregated formulations calculate velocities and pressures in an alternative iterative sequence, requiring much less storing needs than the mixed methods. Moreover, these algorithms not only achieve a greater reduction in the number of equations compared to the penalty method (in this formulation the dimension of the system to be solved is equal to the number of nodes), but also allow for the production of narrow band stiffness matrices, when a proper renumbering of the nodes has been carried out. The segregated method also avoids the use of the sometimes inconvenient penalty parameter.

Another gain of these segregated algorithms is that a mixed-order interpolation can be used. As has already been said, the mixed and penalty methods require a velocity approximation different from that of the pressure. The easier-to-implement discretization of the domain in terms of the same basic functions for both velocity and pressure in connection with this kind of segregated formulations leads to oscillation-free solutions and the tendency to produce the checkerboard pressure distribution is consequently eliminated.

The use of the weighted residuals method on the steady dynamic equation gives the equation

$$\int_\Omega w_i^h(u_j^h u_{i,j}^h - f_i^h)\,\mathrm{d}\Omega + \nu\int_\Omega w_{i,j}^h u_{i,j}^h\,\mathrm{d}\Omega + \int_\Omega w_i^h p_{,i}^h\,\mathrm{d}\Omega - \int_{\Gamma_2} t_i^h w_i^h\,\mathrm{d}\Gamma_2 + \sum_e \int_{\Omega_e} \bar{p}_i^h\left(u_j^h u_{i,j}^h - \nu u_{i,jj}^h + p_{,i}^h - f_i\right)\mathrm{d}\Omega = 0. \tag{12}$$

The matrix version of the dynamic system can be written as

$$\begin{aligned}\mathbf{C}(\mathbf{u},\mathbf{v})\mathbf{u} + \nu\mathbf{A}\mathbf{u} = \mathbf{G}\mathbf{u} &= \mathbf{f}_x - \int_\Omega \overline{w}_i \frac{\partial N_j}{\partial x} p_j\,\mathrm{d}\Omega,\\ \mathbf{C}(\mathbf{u},\mathbf{v})\mathbf{v} + \nu\mathbf{A}\mathbf{v} = \mathbf{G}\mathbf{v} &= \mathbf{f}_y - \int_\Omega \overline{w}_i \frac{\partial N_j}{\partial y} p_j\,\mathrm{d}\Omega,\end{aligned} \tag{13}$$

where the right-hand side member of these equations is considered as a given value and will be taken as zero for the first iteration. We can rewrite now equation (12) as

$$\begin{aligned}g_{ii}u_i &= -\sum_{j\neq i} g_{ij}u_j + f_{xi} - \int_\Omega \overline{w}_i \frac{\partial N_j}{\partial x} p_j\,\mathrm{d}\Omega,\\ g_{ii}v_i &= -\sum_{j\neq i} g_{ij}v_j + f_{yi} - \int_\Omega \overline{w}_i \frac{\partial N_j}{\partial y} p_j\,\mathrm{d}\Omega,\end{aligned} \tag{14}$$

where g_{ij} is the coefficient matrix of the dynamic system. Now we can express the velocities as

$$\begin{aligned}u_i &= \frac{1}{g_{ii}}\left(-\sum_{j\neq i} g_{ij}u_j + f_{xi} - \int_\Omega \overline{w}_i \frac{\partial N_j}{\partial x} p_j\,\mathrm{d}\Omega\right),\\ v_i &= \frac{1}{g_{ii}}\left(-\sum_{j\neq i} g_{ij}v_j + f_{yi} - \int_\Omega \overline{w}_i \frac{\partial N_j}{\partial y} p_j\,\mathrm{d}\Omega\right).\end{aligned} \tag{15}$$

A set of 'intermediate' velocities, the pseudo-velocities $\tilde{u}_i$ and $\tilde{v}_i$, are defined as follows:

$$\tilde{u}_i = \frac{1}{g_{ii}}\left(-\sum_{i\neq j} g_{ij}u_j + f_{xi}\right) \qquad \tilde{v}_i = \frac{1}{g_{ii}}\left(-\sum_{i\neq j} g_{ij}v_j + f_{yi}\right). \tag{16}$$

The velocities can be now approximated in terms of the pseudo-velocities by using the expressions

$$u_i \approx \tilde{u}_i - K_i^p \frac{\partial N_j}{\partial x} p_j; \qquad v_i \approx \tilde{v}_i - K_i^p \frac{\partial N_j}{\partial y} p_j, \tag{17}$$

where the velocity–pressure coupling coefficients K_i^p are given by the equation

$$K_i^p = \frac{1}{g_{ii}}\int_\Omega \overline{w}_i\,\mathrm{d}\Omega. \tag{18}$$

Using the weighted residuals method in the continuity equation we obtain

$$\int_{\Omega_h} w_{i,j}^h u_j^h\,\mathrm{d}\Omega - \int_{\Gamma_2} w_i^h u_j^h n_j^h\,\mathrm{d}\Gamma_2 = 0 \tag{19}$$

or in expanded form

$$\int_{\Omega_h} \frac{\partial w_i}{\partial x} N_k K_k^p \frac{\partial N_j}{\partial x} p_j + \frac{\partial w_i}{\partial y} N_k K_k^p \frac{\partial N_j}{\partial y} p_j\,\mathrm{d}\Omega = \int_{\Omega_h} \frac{\partial w_i}{\partial x} N_j \tilde{u}_j + \frac{\partial w_i}{\partial y} N_j \tilde{v}_j\,\mathrm{d}\Omega - \int_{\Gamma_h} w_i(N_j u_j n_x + N_j v_j n_y)\,\mathrm{d}\Gamma_2. \tag{20}$$

Once the velocity system (13) has been calculated, the pressure system (20) is obtained and solved, the velocities are then corrected by using the following expression:

$$u_i = \tilde{u}_i - \frac{1}{g_{ii}} \int_\Omega \overline{w}_i \frac{\partial N_j}{\partial x} p_j \, d\Omega \qquad v_i = \tilde{v}_i - \frac{1}{g_{ii}} \int_\Omega \overline{w}_i \frac{\partial N_j}{\partial y} p_j \, d\Omega \tag{21}$$

to ensure continuity.

The iterative process is based upon assuming a zero pressure field as a first guess in the resolution of the dynamic equation, providing the velocity field as the output. Once the pseudo-velocities (16) and the pressure–velocity coupling coefficients (18) have been calculated, the continuity system (20) is assembled and solved, and thus the values for the pressure field are obtained. Finally, the velocities are updated, making use of the newly determined pressure field (21), and with both the new velocities and pressures the dynamic equations are reassembled, solved and the same procedure is repeated until convergence is achieved.

When employing a segregated algorithm, the use of uncoupled velocity and pressure fields may lead to the divergence of the whole process. To avoid this problem, an under-relaxation of the unknowns can be introduced so as to guarantee the convergence of the process. The momentum equations are also under-relaxed making use of an inertial relaxation factor r_i defined as

$$r_i = \int_\Omega w_i \, d\Omega \tag{22}$$

with r_i being added to the terms in the diagonal of the dynamic coefficient matrix as follows:

$$\begin{aligned} (g_{ii} + r_i)u_i^n + \sum_{j \neq i} g_{ij} u_j^n &= f_{xi} - \int_\Omega \overline{w}_i \frac{\partial N_j}{\partial x} p_j \, d\Omega + r_i u_i^{n-1}, \\ (g_{ii} + r_i)v_i^n + \sum_{j \neq i} g_{ij} v_j^n &= f_{yi} - \int_\Omega \overline{w}_i \frac{\partial N_j}{\partial y} p_j \, d\Omega + r_i v_i^{n-1} \end{aligned} \tag{23}$$

with u_i^{n-1} and v_i^{n-1} being the values of the velocities obtained in the previous iteration.

The use of this formulation, leads to a N-dimensioned narrow band coefficient matrix, and consequently to further memory savings in the resolution of the Navier–Stokes equations.

3.4. Shallow water formulation

Although any of the previously explained types of finite elements formulations could be used in the implementation of the shallow water equations, we will only present here the mixed formulation. The mixed finite element approach will share the same advantages and shortcomings of that of the laminar mixed formulation explained before. If we apply the weighted residuals method on both the dynamic and continuity shallow water equations, we obtain

$$\begin{aligned} &\int_{\Omega_h} w_i^h (u_{i,t}^h + u_j^h u_{i,j}^h - g(S_{0i}^h - S_{fi}^h)) \, d\Omega + \nu \int_{\Omega_h} w_{i,j}^h u_{i,j}^h \, d\Omega - g \int_{\Omega_h} w_{i,i}^h h^h \, d\Omega \\ &\quad - \int_{\Gamma_2^n} t_i^h w_i^h \, d\Gamma_2 + \sum_e \int_{\Omega_e} \bar{p}_i^h (u_{i,t}^h + u_j^h u_{i,j}^h - \nu u_{i,jj}^h + g h_{,i}^h - g(S_{0i}^h - S_{fi}^h)) \, d\Omega = 0, \\ &\int_{\Omega_h} q^h (h_{,t}^h + h^h u_{i,i}^h + u_i^h h_{,i}^h) \, d\Omega = 0. \end{aligned} \tag{24}$$

But now we have a new difficulty that did not appear in the numerical approach to the 2D Navier–Stokes equations presented previously: we have the depth itself and the gradient of depth being included as part of the continuity equation. In fact, the inclusion of the depth and the gradient of depth in the continuity equation, allows for the verification of the conservation of mass in a pseudo-3D basis and not on a 2D laminar sense, as a consequence of having carried out an integration in depth of the Navier–Stokes

equations. As a consequence, some pseudo-non-linearities show up in the continuity equation, which should be considered in addition to the non-linearities resulting from the convective quadratic term. The shallow water equations will be integrated in order to cope with this problem.

Let us introduce the following approach: we are going to assume that the depth values in the continuity equation are going to be constant all over the domain for the first iteration, and equal to the outflow given depth. In the following iterations carried out in order to solve the convection, the depths and gradients of depth in the continuity equation will be evaluated from the results of the former iteration, and this evaluation will be carried out in terms of a finite difference approach. Since a non-equal order interpolation of the unknowns must be used to achieve converge, the velocities and the depths are calculated on a different mesh. The depths to be re-fed in the continuity equation for the second and the following iterations are going to be evaluated on the velocity mesh points. Recall that the basic element used in this formulation is the Q1P0 basic element, or in other words, the velocity is interpolated in terms of bilinear continuous functions with respect to a four-nodded basic element, and the depth is interpolated in terms of constant discontinuous functions within the basic element. The depth at a velocity node h_i^* will be taken as the mean value of the depths for the former iteration in the surrounding basic elements, and the gradients of depth on the velocity mesh $\dot{\mathbf{h}}^*$, will be evaluated from the star depths h_i^* on a finite difference basis. For more details see [43].

After each iteration for convection has been solved, the star depths and star gradients of depth are calculated and re-fed into the continuity equation. The use of this algorithm developed by the authors in the resolution of the shallow water equations achieves very good numerical results as will be seen in the numerical examples. The general procedure for the obtaining of the system of differential equations could be written in its matrix form as

$$\begin{aligned} &\mathbf{M}_{\upsilon}\frac{\partial \underline{\upsilon}}{\partial t}+\mathbf{C}_{\upsilon}(\mathbf{u},\mathbf{v})\underline{\upsilon}+\nu\mathbf{A}_{\upsilon}\underline{\upsilon}-\mathbf{B}\mathbf{h}=\mathbf{f},\\ &\mathbf{D}(\mathbf{h}^*)\underline{\upsilon}+\mathbf{E}(\dot{\mathbf{h}}^*)\underline{\upsilon}=\mathbf{0}, \end{aligned} \tag{25}$$

where $\mathbf{M}_{\upsilon}$ is the mass matrix, t is the time, $\mathbf{C}_{\upsilon}(\mathbf{u},\mathbf{v})$ is the convective matrix, $\mathbf{A}_{\upsilon}$ is the viscous matrix, $\mathbf{B}$ is the depth matrix, $\mathbf{f}$ is external forces vector, $\mathbf{D}(\mathbf{h}^*)$ is the star depth matrix, $\mathbf{E}(\dot{\mathbf{h}}^*)$ is the star gradient of depth matrix, $\mathbf{f}$ is the external forces vector, $\mathbf{h}$ is the depth vector and $\underline{\upsilon}$ is the velocity vector.

3.5. SUPG stabilization of the algorithms

The above formulations include a SUPG term in the dynamic weighting functions. This SUPG contribution will affect all the terms in the dynamic equation and will be based upon an optimal rule function for the obtaining of the multi-dimensional diffusion coefficient. The SUPG formulation will be the following:

$$\overline{w}_i = w_i + \bar{p}_i \quad \text{with} \quad \bar{p}_i^h = \frac{\bar{k}\hat{u}_j^h w_{i,j}^h}{\|\mathbf{u}^h\|} \quad \hat{u}_i = \frac{u_i}{\|\mathbf{u}\|} \quad \|\mathbf{u}\|^2 = u_i u_i, \tag{26}$$

where the multi-dimensional definition of the diffusion coefficient $\bar{k}$ is given by

$$\bar{k} = \frac{\bar{\xi}u_{\xi}^h h_{\xi} + \bar{\eta}u_{\eta}^h h_{\eta}}{2}, \tag{27}$$

where

$$\begin{aligned} &\bar{\xi} = \left(\coth\alpha_{\xi} - \frac{1}{\alpha_{\xi}}\right) \quad \bar{\eta} = \left(\coth\alpha_{\eta} - \frac{1}{\alpha_{\eta}}\right)\\ &\alpha_{\xi} = \frac{u_{\xi}^h h_{\xi}}{2\nu} \qquad \alpha_{\eta} = \frac{u_{\eta}^h h_{\eta}}{2\nu}\\ &u_{\xi}^h = e_{\xi i}u_{ei}^h \qquad u_{\eta}^h = e_{\eta i}u_{ei}^h, \end{aligned} \tag{28}$$

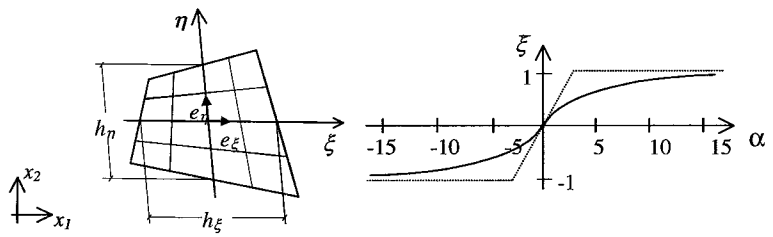

Fig. 1. Characteristic basic-element lengths and unit vectors. Optimal rule for the approximation of $\bar{\xi}$ and $\bar{\eta}$.

where h_ξ, h_η and $e_{\xi i}$, $e_{\eta i}$ are the characteristic basic-element lengths and unit vectors in the direction of the local axes ξ and η (see Fig. 1). The parameters α_ξ and α_η are the directional Reynolds numbers of the basic element, u^h_{ei} is the velocity in the interior of the element and ν is the kinematic viscosity of the fluid. Different versions of the streamline upwind formulation have been used by other authors and can be found in [9,12,35,48]. For the present work, the stabilization technique will be based upon the SUPG weighting functions as defined in (26)–(28). These weighting functions will be applied on the formulation as specified in formulas (5), (9), (12) and (24), with very good results as will be seen in the numerical examples shown in the following section.

4. Benchmark numerical results

Once we have presented the algorithms to be used in this work, we are going to proceed to validate them by using the cavity flow and the Backward-facing step benchmark problems.

4.1. The cavity flow benchmark problem

The driven cavity flow is a classical test used by many authors to check the quality of the methodology employed in the resolution of the 2D Navier–Stokes equations. This benchmark problem is based upon the analysis of the flow in a square cavity with prescribed horizontal velocity in the upper side and solid boundaries in the lateral and bottom sides. This is a challenging problem due to the presence of several re-circulating regions in which the solution changes rapidly, and because of the pressure singularities that show up in the upper corners.

This benchmark test will be used, to validate the algorithms developed in this thesis by its comparison with the results obtained by other authors. These results to compare with, will be those of Ghia et al. [14] obtained by employing a mesh of 129 × 129 nodes; Hannani et al. [15] with non-uniform meshes of 32 × 32, 45 × 45 and 80 × 80 Q1P0 basic elements; and the results by Kondo [27], making use of a 40 × 40 element mesh of four-node, non-regular basic elements. All of them can be considered as reference results, specially those of Ghia et al., that are commonly employed to check the validity of the algorithms by most of the authors in the related bibliography.

The boundary conditions used for this problem have been of the Dirichlet type in all the boundaries. A unitary horizontal velocity heading towards the right-hand side has been prescribed for the top side (including the upper corners), and the no-slip condition has been considered for the rest of the boundary. The discretized domain used in the calculations has been a 1681-node non-regular mesh with 1600 Q1P0 elements (see Fig. 2).

The results for all the formulations considered have been the same and can be seen in Figs. 3–6. This benchmark problem has been solved by making use of the mixed, penalty and segregated algorithms and

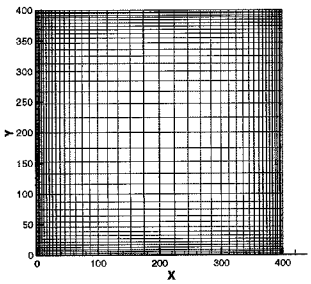

Fig. 2. Cavity flow 41 × 41 non-regular mesh.

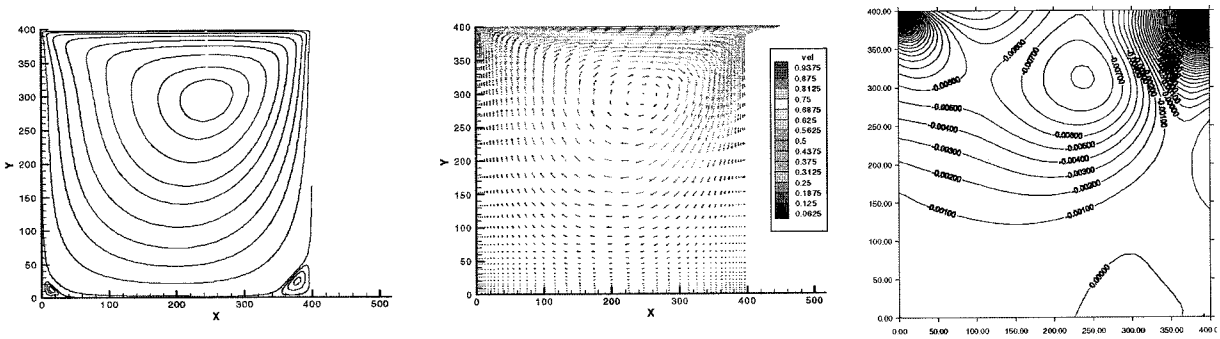

Fig. 3. Cavity flow: velocity field, streamlines, and pressure field $Re = 100$.

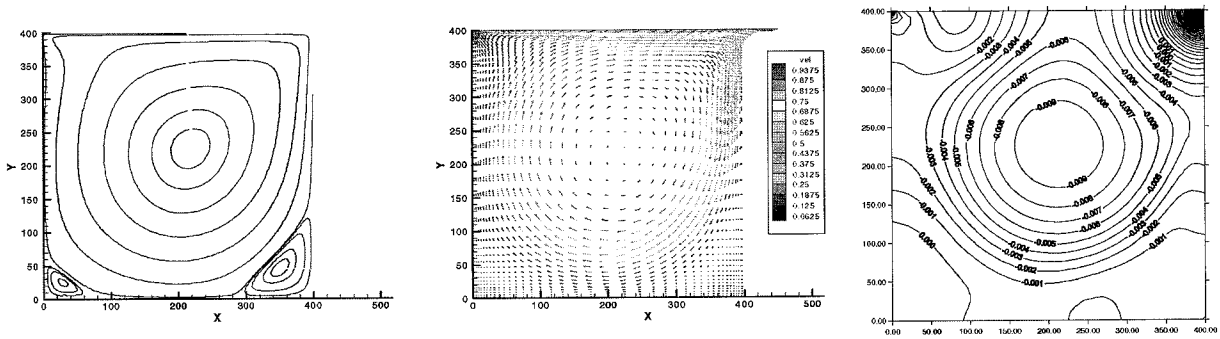

Fig. 4. Cavity flow: velocity field, streamlines, and pressure field $Re = 1000$.

the Reynolds numbers used have been 100, 1000, 5000 and 10 000. The Reynolds number has been defined as $Re = UL/v$, where U is the velocity in the upper side, L is the length of the side of the square domain, and v is the kinematic viscosity. The value of Reynolds = 10 000 is considered as a limit for the steady cavity flow calculations, since it has been shown through detailed numerical experiments [37] that above this bound, the stationary solution ceases to be stable.

The most commonly used comparison results for this benchmark problem are the horizontal velocities along a central vertical line, which have been plotted in Figs. 7 and 8.

The horizontal velocity profiles along a central vertical line adjust to the reference values of [14], with a much finer mesh and are also substantially better than those of [15] and [27], for a mesh with a similar

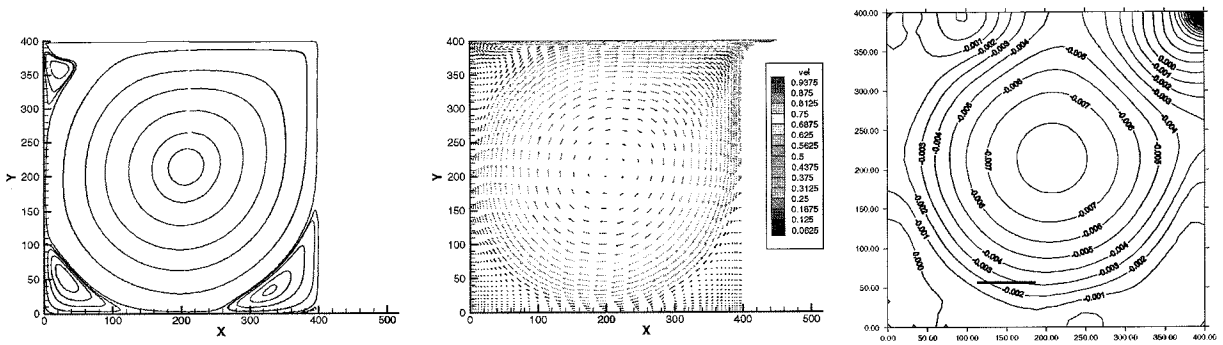

Fig. 5. Cavity flow: velocity field, streamlines, and pressure field $Re = 5000$.

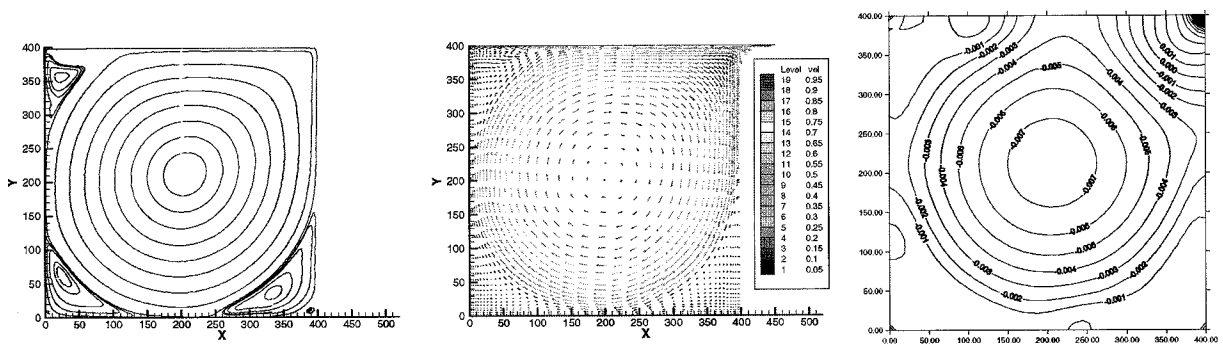

Fig. 6. Cavity flow: velocity field, streamlines, and pressure field $Re = 10000$.

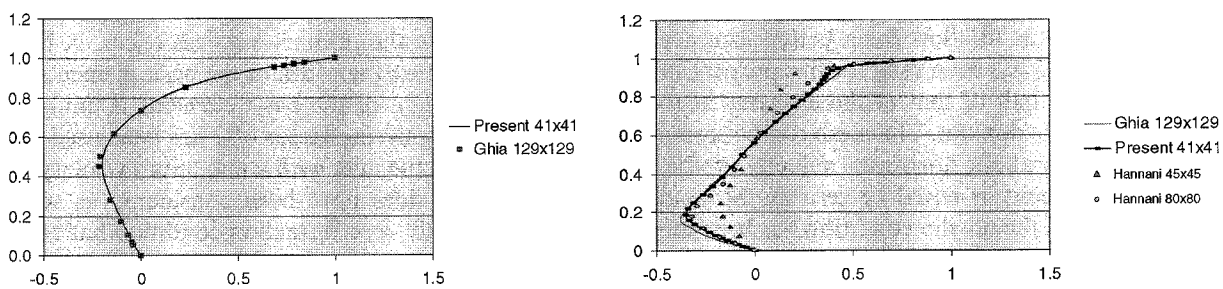

Fig. 7. Horizontal velocities along a central vertical line for $Re = 100$, and 1000.

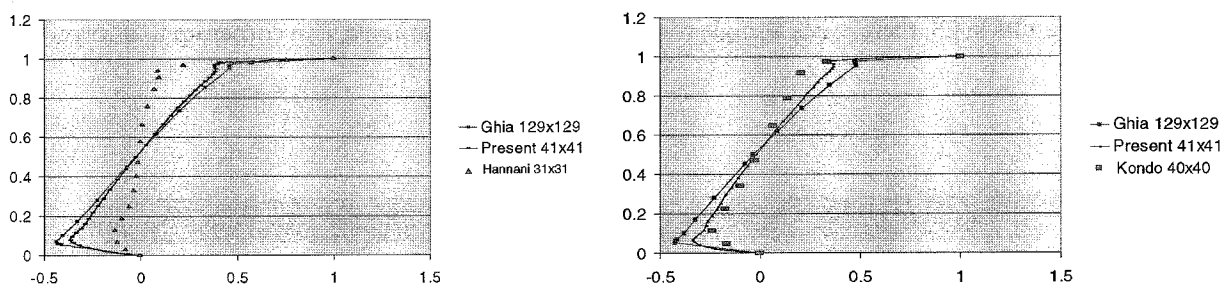

Fig. 8. Horizontal velocities along a central vertical line for $Re = 5000$, and 10000.

refinement and even a finer one. No substantial differences are observed among the results of the three formulations used for the velocity field results nor for the pressure field results, which are also in good agreement with the benchmark solutions of the problem obtained by those authors.

The good results obtained in the velocity profiles have made useless the employment of a finer mesh, which would necessitate a much longer CPU time. The calculation times are shorter for the mixed algorithm and of increasing magnitude for the penalty and segregated method. For the penalty solution, the introduction of the penalty parameter makes the linear system of equations more difficult to be solve, since the penalty parameter tends to zero. This computational time can be reduced, anyhow, by the use of a properly weighted penalty parameter.

The algorithms implemented have proved to give very accurate results even for a less refined mesh, showing that the upwind weighting implemented in the numerical scheme is a powerful tool to solve some flow problems without using very refined meshes, and with no wiggles in the so-obtained solution.

4.2. The backward-facing step benchmark problem

The laminar Backward Facing Step benchmark problem is presented next, as one of the most commonly used benchmark problems in the literature, in order to validate the algorithms that give solution to the Navier–Stokes equations. The backward step is based upon a simple geometry where flow separation and reattachment occur. Experimental data for this problem can be found in [2], who also solved this problem numerically by using a control-volume-based finite difference method. The problem of the backward step flow will be solved in this section by using the penalty algorithm and its results will be compared with those of Armaly et al., which are generally used as verification data.

The geometry and boundary conditions considered for this benchmark problem have been those used in [2]. An expansion ratio of 1:1.94 has been considered for the widening of the channel, which has a total length of 50 so as to allow for the vortices to take place. The inlet boundary has been located at 3.5 step heights upstream of the expansion corner. The domain has been split into 2850 Q1P0 basic non-regular elements with 3021 nodes. The mesh is coarser at the outlet and more refined at the left-hand side of the channel, so as to allow for a better accuracy in the regions where the primary vortices occur. A bias parameter of 0.5 has been used for this purpose along the x-axis, therefore the width of the basic elements at the inlet is one half of that of the elements at the outlet, and the height of the basic elements is uniform within the whole domain. The mesh can be seen in Fig. 9, where a magnifying factor of 2 has been used for the y-axis. A parabolic horizontal velocity profile has been imposed at the inlet with a maximum velocity of 1, and the velocity is equal to zero at the boundaries. The lateral sides have been considered as solid boundaries and the no-slip condition has been imposed on them. Finally, a zero traction condition has been imposed at the outlet.

The flow has been obtained for a Reynolds number between 100 and 1200 (Figs. 10–12). The Reynolds number has been defined as $Re = uD/v$, where u is the average inlet velocity, D is the hydraulic diameter and the kinematic viscosity v has been altered so as to make the Reynolds number vary. As foretold by the experimental results in [2], there exists a single re-circulation zone at the expansion corner up to a Reynolds

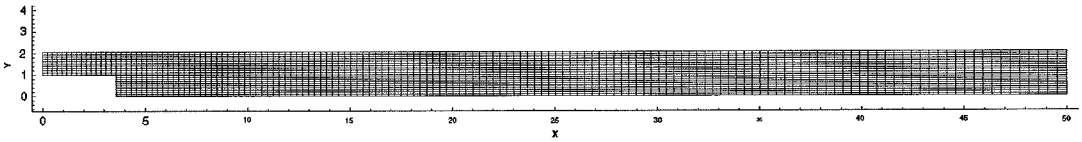

Fig. 9. Backward facing step—mesh.

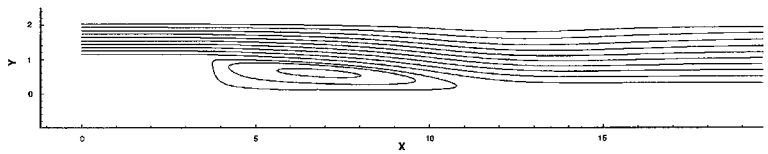

Fig. 10. Flow in a backward facing step, streamlines for $Re = 400$.

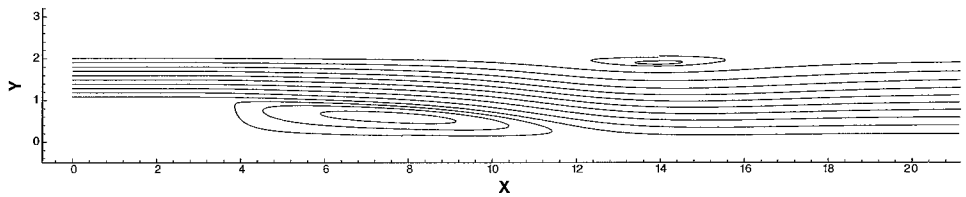

Fig. 11. Flow in a backward facing step, streamlines for $Re = 500$.

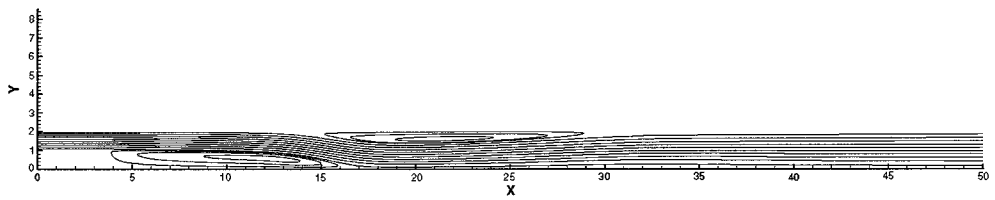

Fig. 12. Flow in a backward facing step, streamlines for $Re = 1200$.

number of about 450, beyond which a second vortex shows up at the top boundary, and gets bigger as the Reynolds number is increased.

The size of the reattachment zones s_i versus the Reynolds number is compared with the experimental and numerical results by Armaly; these results can be seen in Figs. 14–16. The reattachment locations of the vortices are defined as follows; s_1 is the reattachment location of the primary vortex, s_2 is the separation location of the secondary top boundary vortex and s_3 is the reattachment location of the secondary vortex. All of them have been measured from the expansion corner, as depicted in Fig. 13.

As seen in Figs. 14–16, the computed results obtained in the present work compare more favourably with experimental data than the numerical results from Armaly. Although the present results are totally analogous to the experimental data in [2] for s_3 and for all the Reynolds numbers considered, when taking about s_2 and specially s_1, the experimental data differ from the calculated results beyond a Reynolds number of about 400. This difference between measured and calculated values is not only shown in the numerical results by Armaly et al., but also in the results by Kim [26] among many others. The differences in these values are due to the fact that the 3D effect becomes very important as the Reynolds number is increased. As pointed out by Armaly, these effects became predominant beyond a Reynolds number of 1300.

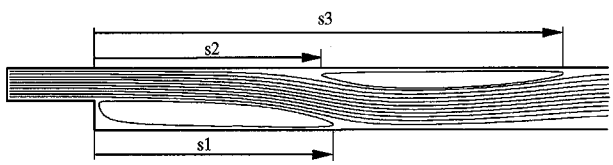

Fig. 13. Flow over a backward facing step: sketch of the recirculation lengths s_i.

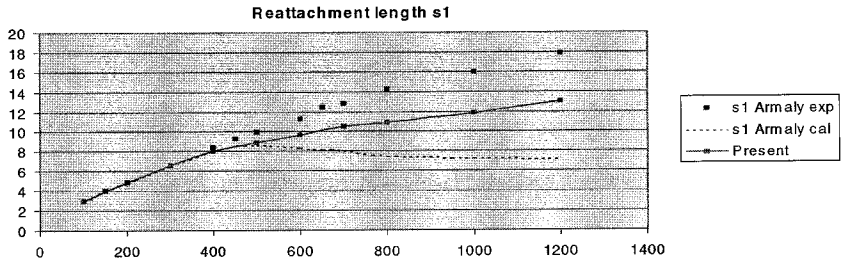

Fig. 14. Reattachment length s_1 versus Reynolds number for the backward facing step.

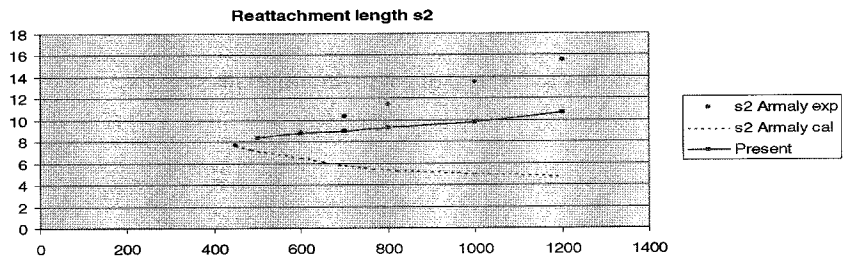

Fig. 15. Reattachment length s_2 versus Reynolds number for the backward facing step.

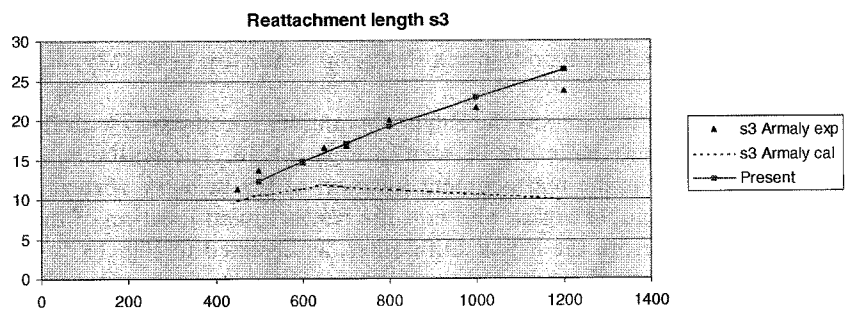

Fig. 16. Reattachment length s_3 versus Reynolds number for the backward facing step.

5. Application to some wastewater treatment problems

Once the code has been checked on some well-known benchmark problems with optimum results, it has been used to solve some real flow problems related with the civil engineering technology and in particular with the wastewater treatment industry.

Some authors have used the potential flow equations to evaluate the flow in clarifiers and other wastewater treatment basins. When we use these simplifications, we can obtain an approximation of the flow for slow creeping conditions, but only the resolution of the all-term-including Navier–Stokes equations will allow us to detect the real streamlines and the vortices that show up even for very slow water flows. Let us now use the previously explained formulations in the resolution of the flow in some wastewater treatment basins.

5.1. Flow in a water distribution chamber

The flow that takes place in a chamber that splits the incoming flow of water into three different outlets is observed. This type of water distribution basins can be commonly found in many hydraulic plants.

Let us regard the problem of a cavity in which we had a normal lateral inflow to be split into three outflows, one of them on the opposite side (exit number 3 in Fig. 17) and the other two on the adjacent sides (exits 1 and 2). A wall is placed between outlets one and two so as to observe the influence of this structure in the distribution of the water flow. A typology similar to this one can be found in many water distribution tanks in wastewater treatment plants [1].

The geometry used for this simulation has been a rectangular domain 400 cm high and 300 cm wide, split into a regular 1200-node mesh with 1131 basic Q1/P0 elements. The inflow channel and outlet number 3 have a width of 100 cm, whereas outlets 1 and 2 spread over the whole bottom side. The distribution wall is placed on abscise 145 cm and has a height of 100 cm. These geometrical proportions are similar to those found in a conventional chamber for distributing a single wastewater flow among three different outlets, such as those used in the *As Pontes* treatment plant (powered by ENDESA).

A unitary, normal and constant inflow is considered at the inlet. The no-slip condition has been imposed on the solid boundaries and the velocity at the outlets has been considered as an unknown and a zero-traction condition has been imposed on it. The flow has been solved for a Reynolds number that takes the value of 30, 60, 100 and 300 and the results can be seen in Figs. 18 and 19. The Reynolds number has been taken as the quotient of the inflow velocity times the width of the rectangle over the kinematic viscosity of the fluid.

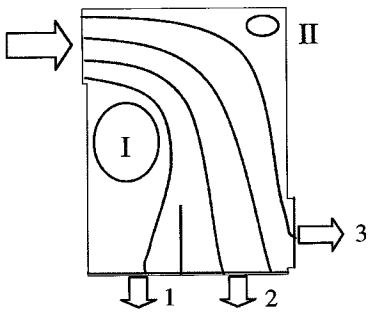

Fig. 17. Flow in a water distribution chamber, sketch of the chamber.

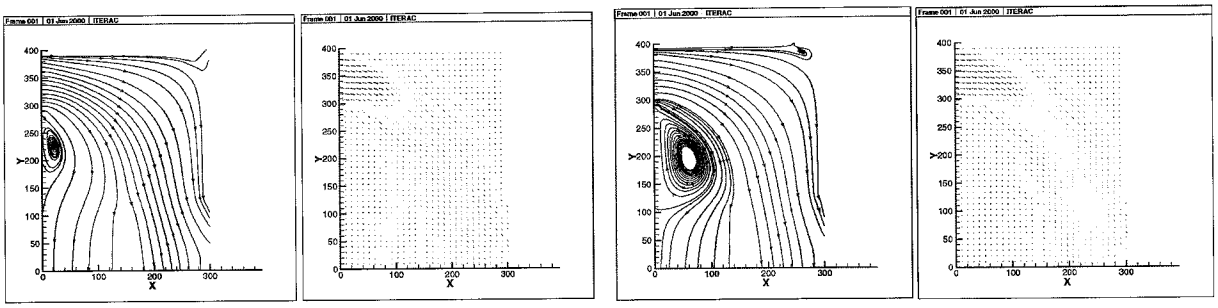

Fig. 18. Flow in a distribution chamber, streamlines and velocities for *Re* 30 and 60.

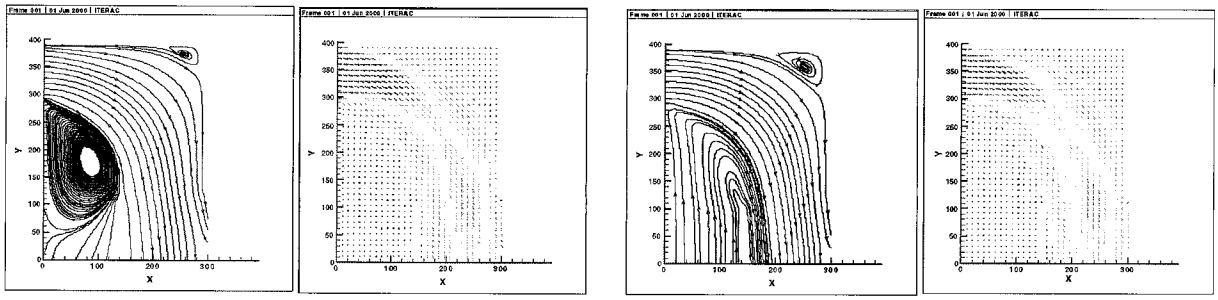

Fig. 19. Flow in a distribution chamber, streamlines and velocities for *Re* 100 and 300.

The primary vortex (see Fig. 17), shows up for the flow featured by a Reynolds number of 30. In this case, the secondary vortex is not yet well formed. With the increasing value of the Reynolds number, vortices I and II are progressively developed and vortex I happens to 'obstruct' the outlet number 1. For the largest Reynolds number considered, the flow turns to head inwards in gate number one.

The results obtained for the flow cases considered are in good agreement with the hydraulic behaviour of the chamber as can be seen in the experimental results obtained for a similar scale model of a distribution basin, carried out in the Escuela Técnica Superior de Ingenieros de Caminos, Canales y Puertos de La Coruña [5].

Fig. 20 shows the vertical component of the velocity for outlets one and two and the horizontal component for outlet three. In the first plot we can see how the vertical component of the flow coming out of gate one, gets smaller as the Reynolds number is increased, up to a point in which the direction of the flow is inverted, when the primary vortex happens to reach the splitting wall. Meanwhile, the flow going out through outlet number two is progressively increased as the Reynolds gets bigger, and in outlet number three the flow is sent towards the lower side of the gate.

In all the calculations carried out up to this point, no contributions have been added to the source term in order to account for the energy losses caused by the friction with the boundary. For the following calculations a Manning coefficient equal to 2.5×10^{-3}, 5×10^{-3}, and 7.5×10^{-3} $cm^{-1/3}s$ has been used, where the last of those corresponds to a smooth concrete bed. All the computations have been carried out for a Reynolds number of 100. For this Reynolds number the primary vortex is well formed and therefore the decrease in its size can be more easily observed as the Manning coefficient is increased. The results for this analysis are shown in Fig. 21.

As it can be seen from the plots, the effects of considering the friction with the bed are similar to the energy losses caused by the consideration of a bigger viscosity, and consequently the imposition of a greater

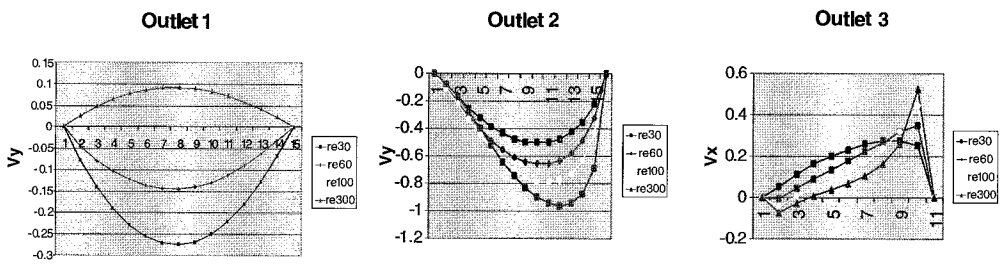

Fig. 20. Vertical, vertical and horizontal components of the velocity through gates 1, 2 and 3 for Reynolds numbers 30, 60, 100 and 300.

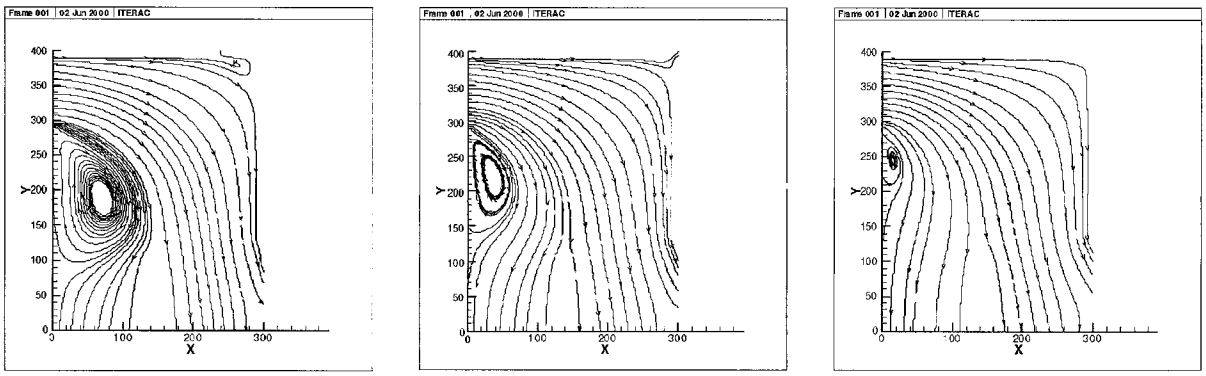

Fig. 21. Flow an a distribution chamber. Streamlines for $n = 2.5 \times 10^{-3}$, 5.0×10^{-3}, and 7.5×10^{-3} $\mathrm{cm}^{-1/3}$ s ($Re = 100$).

friction among particles. As a result, the streamline map of the flow for the harder roughness conditions, is similar to the one obtained for $Re = 30$ instead of 100. As a conclusion, the consideration of the Manning term, gives a more practical evaluation of the energy losses taking place in a real flow, which as explained before allows for the consideration of the turbulent effects as a whole and is in good agreement with the experimental results by [5].

The analysis of the flow distribution in the chamber can give a hint on the designing of the basin. The so-defined geometry results in the appearance of two energy dissipating vortices, which get bigger as the Reynolds number is increased. The appearance of these recirculation zones can be a wanted feature in order to dissipate some energy, and allow for particle settlement in these zones. On the contrary for some other purposes it can be an unwanted effect that happens to obstruct the left-hand side outlet, resulting in an unequal distribution among the three outlets. Anyway, the numerical evaluation of the flow in the chamber, forecasting the behaviour of the water, is without any doubt a powerful tool for its designing.

5.2. Flow in rectangular and circular clarification basins

In this section, the flow of water in a rectangular and circular conventional clarification basins has been considered. Clarification has two main applications in the water treatment processes. Its most usual aim is to reduce the solids load after coagulation and flocculation have taken place. Its second application is the removal of heavy settleable solids from a turbid source to lessen the solids load in water. The aim of a good clarification basin design is the obtaining of a sufficiently stable flow, so as to achieve a better sedimentation. There is a large number of non-conventional devices for high rate clarification, such as tube or plate settlers, dissolved air flotation clarifiers, sludge blanket or slurry recirculation clarifiers. The choice of one of those depends on the features of the inflow water, the outflow water requirements, time, space and budget availability to carry out the purification of the water. The description of the flow may be a powerful tool to attain an optimum shape in the designing of these structures, in order to make the most of the plant resources.

The rectangular and circular basins are the most commonly used clarification devices. In spite of their simplicity, they have achieved excellent results with scant maintenance costs. These basins were originally designed with the capacity to store sludge for several months and were periodically taken out of service for manual cleaning. Today, most of the clarification basins include a continuous cleaning mechanical equipment, such as dragging chains that plow the sludge along the basin floor to hoppers. Nevertheless, these mobile devices for cleaning and other purposes do not have an important influence in the streamline distribution, and can be ignored when the flow is calculated (for further details on clarification basins you

can refer to [30]). We are going to evaluate the flow features in the vertical section of a rectangular and circular clarifiers, with the following dimensions and design parameters:

Clarifier	Dimensions (m)	Depth (m)	Slope (%)	Nodes and elements	Detention time (h)	Surface load rate (m/h)
Rectangular	W: 9, L: 24	3.3	1.2	1052, 949	3	1
Circular	D: 17.5	3.65	0.8	817 × 2, 756 × 2	3	1

When working with clarifying basins, one of the criteria to be used in their definition is that of achieving a maximum head loss at the inlet, so as not to disturb the slow flow of the water mass being treated. Therefore, we should avoid turbulence by placing some kind of energy dissipating structure in the faster zone, that is the inlet (see Fig. 22). One of these maze-looking dissipating structures has been considered for the inlet of our clarifiers, being placed in the left-hand side for the rectangular one and in the centre of the basin for the circular, where the respective inlets are. For the outlets (in the right-hand side for the rectangular one and in the perimeter for the circular one), a conventional overflow launder has been disposed. The domain in which the flow takes place has been split into 949 Q1P0 basic elements with 1052 nodes for the rectangular and 817 × 2 nodes and 756 × 2 elements for the circular, which has benefited from its symmetry property. For the working parameters chosen, a velocity of 1 cm/s has been imposed at the inlet in both of them. The no-slip condition has been imposed at the bottom and lateral sides, and the spillway has been left free with a zero-traction boundary condition. For the topside, the vertical velocity has been fixed as zero and the horizontal velocity has been left free. The results for the velocity and pressure fields can be seen in Figs. 23 and 24.

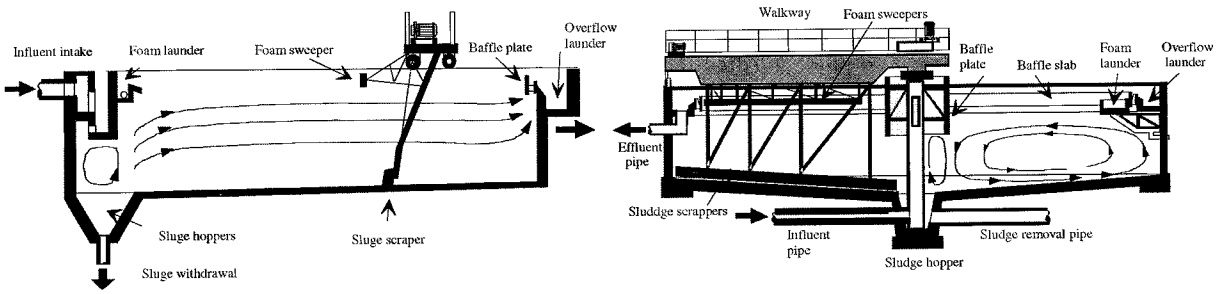

Fig. 22. Rectangular and circular clarifier with bottom sludge scraper—sketch.

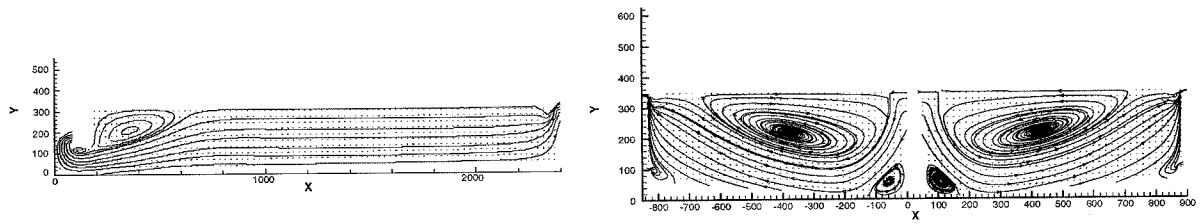

Fig. 23. Flow in a rectangular and circular clarifying basin—streamlines.

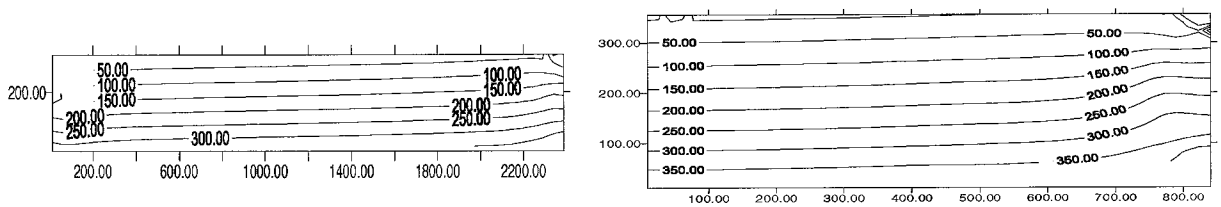

Fig. 24. Flow in a rectangular and circular clarifying basin—pressures.

6. Conclusions

In this work, an exhaustive analysis of the incompressible flow has been carried out, from the very definition of the governing equations, up to the resolution of some practical problems, passing through the comprehensive study of the numerical techniques used in their resolution. As a direct consequence of this study, a code has been written based upon this analysis, which allows for a modelling of the incompressible flow based upon a realistic interpretation of the forces taking place within the flow, and giving optimum results.

The three different approaches: mixed, penalty and segregated, have been implemented and their results have been checked and verified by the comparison of the three of them among themselves and also against some reference results. As a consequence, several conclusions have been reached. The first is that, as expected, the results obtained by the three of them in the resolution of some benchmark problems have been identical, in a comparison study that had not been carried out prior to this work. The algorithm used does not affect the accuracy of the solutions when an adequate selection of the numerical parameters has been carried out. The second conclusion is that all the results compare very favourably with the reference numerical and empirical results by other authors. As a consequence, the code not only enables a comparison study of the available finite element numerical techniques for the resolution of the Navier–Stokes equations, but also, as proved by the examples provided, contributes to a better and faster approach to these problems.

A newly developed algorithm for the resolution of the shallow water equation, making use of the finite difference tools within the finite element frame, has been implemented with optimum results. The evaluation of this friction term is based upon on a Manning type formula, which makes use of the empirically determined Manning roughness coefficient. This term accounts not only for the energy losses that take place because of the friction with the wetted perimeter, but also for the overall turbulent losses that take place over the whole domain of integration. The turbulent eddies taking place within the flow are not detected, but the turbulent energy losses are taken into account thanks to this empirically determined formula, which provides a meaningful solution for practical flows.

Some of the most commonly used hydrodynamic models for the flow calculations, incorporate a turbulence model featured by a constant eddy viscosity, which is not hydraulically speaking well justified. In contrast, the shallow water algorithm developed by the author includes an empirically determined turbulent losses term but also keeps the Navier–Stokes formulation of the problem, being ready to incorporate a two-equations turbulence model that has been developed within the research group and provides an eddy viscosity that varies in time and space.

The accuracy of the numerical solutions so-obtained has been checked by using some reference benchmark numerical and empirical solutions with great success, and once the program has been validated, it has been used in the resolution of some wastewater treatment flow problems. The so defined code creates an optimum frame for the evaluation of the flow in some wastewater treatment basins, which is an essential tool in the designing of the wastewater treatment plants for the optimization of their behaviour. The

evaluation of the pressure and velocity of the flow in these basins provides very useful information about the flow properties. The data about the streamlines and velocity field distribution allows us to know where the main recirculation regions are taking place. This information will be priceless for the purpose of obtaining the geometrical parameters of the basins in order to achieve a better performance for the treatment plant. The obtaining of this optimum geometry will allow for a further recirculation, if the energy losses are required; or will enable its avoidance if unwanted, modifying in this way the detention times within the basin. The velocity and pressure fields also provide invaluable information about the distribution of the discharge among the outlets, which again can be redefined in order to improve the behaviour of the plant. Thanks to the information obtained by this numerical evaluation of the flow, the water treatment basins and channels can consequently be designed to fit the requirements of the processes being carried out.

Acknowledgements

The authors want to express their gratitude to the Environmental Engineering Area of the Civil Engineering School of La Coruña (*Área de Ingeniería Sanitaria y Ambiental de la ETS de Ingenieros de Caminos, Canales y Puertos de La Coruña*), led by Dr. Joaquín Suárez. This work has also been partially funded by the European Union FEDER project '*Optimización de circuitos hidrodinámicos y de los procesos en instalaciones de tratamiento físico-químico de agua. Aplicación a la planta de efluentes químicos de As Pontes*' (1FD1997-0053/HID1,XI/98-X/01), the Foundation of Civil Engineering of Galicia (*Fundación de la Ingeniería Civil de Galicia*), the Ministry of Science and Technology (*Ministerio de Ciencia y Tecnología*), the Regional Government of Galicia (Secretária Xeral de I+D de la Xunta de Galicia) and the private company ENDESA.

References

[1] American Water Works Association, American Society of Civil Engineers, Water Treatment Plant Design, McGraw-Hill, 1988.
[2] B.F. Armaly, F. Durst, J.C.F. Pereira, B. Schönung, Experimental and theoretical investigation of backward-facing step flow, J. Fluid Mech. 127 (1983) 473–496.
[3] I. Babuska, Error bounds for finite element method, Numer. Mathemat. 16 (1971) 322–333.
[4] A.C. Benim, W. Zinser, A segregated formulation of Navier–Stokes equations with finite elements, Comput. Methods Appl. Mech. Engrg. 57 (1986) 223–237.
[5] J. Bonillo, Cálculos hidrodinámicos y de transporte de sustancias solubles para flujos turbulentos en lámina libre, Tesis doctoral, Universidad de La Coruña, 2000.
[6] F. Brezzi, On the existence uniqueness and approximation of saddle point problems arising from Lagrange multipliers. Rev. Française Automatique Informatique Reserche Operationnelle, Ser. Rouge Anal. Numér. 8 (R2) (1974) 129–151.
[7] A.N. Brooks, J.R. Hughes, Streamline upwind/Petrov–Galerkin formulations for convection dominated flows with particular emphasis on the incompressible Navier–Stokes equations, Comput. Methods Appl. Mech. Engrg 32 (1982) 199–259.
[8] G. Carey, J. Oden, Finite Elements, Prentice-Hall, 1984.
[9] H.G. Choi, J.Y. Yoo, Streamline upwind scheme for the segregated formulation of the Navier–Stokes equation, Numer. Heat Transfer 25 (Part B) (1994) 145–161.
[10] R. Codina, An iterative penalty method for the finite element solution of the stationary Navier–Stokes equations, Centro Internacional de Métodos Numéricos Ingeniería, CIMNE, 1991, p. 12.
[11] J. Donea, S. Giuliani, H. Laval, Finite element solution of the unsteady Navier–Stokes equation by a fractional step method, Comput. Methods Appl. Mech. Engrg. 30 (1982) 53–73.
[12] L.P. Franca, S.L. Frey, Stabilized finite element methods. II. The incompressible Navier–Stokes equations, Comput. Methods Appl. Mech. Engrg. 99 (1992) 209–233.
[13] D.K. Gartling, Finite element analysis of viscous incompressible flow, Ph.D. dissertation, University of Texas at Austin, Austin, 1974.
[14] U. Ghia, K.N. Ghia, C.T. Shin, High Re solutions for incompressible flow using the Navier–Stokes equation and the multigrid method, J. Comput. Phys. 48 (1982) 387–411.

[15] S.K. Hannani, M. Stanislas, P. Dupont, Incompressible Navier–Stokes computations with SUPG and GLS formulations—A comparison study, Comput. Methods Appl. Mech. Engrg. 124 (1995) 153–170.
[16] S.K. Hannani, M. Stanislas, Incompressible turbulent flow simulation using a Galerkin/least-squares formulation and a low Reynolds number k–ε model, Comput. Methods Appl. Mech. Engrg. 181 (1–3) (2000) 107–116.
[17] J.C. Heinrich, P.S. Huyakorn, A.R. Mitchell, O.C. Zienkiewicz, An upwind finite element scheme for the two dimensional convective transport equation, Int. J. Numer. Meth. Engrg. 11 (1977) 131–143.
[18] J.C. Heinrich, O.C. Zienkiewicz, Quadratic finite element schemes for two dimensional convective transport problem, Int. J. Numer. Meth. Engrg. 11 (1977) 1831–1844.
[19] J.C. Heinrich, R.S. Marshall, Viscous incompressible flow by a penalty function finite element method, Comput. Fluids 9 (1981) 73–83.
[20] T.J.R. Hughes, W.K. Liu, A. Brooks, Review of finite element analysis of incompressible viscous flow by the penalty function formulation, J. Comput. Phys. 30 (1979) 1–60.
[21] T.R.J. Hughes, A. Brooks, A multidimensional upwind scheme with no crosswind diffusion, in: T.J.R. Hughe (Ed.), Finite Element Methods for Convection Dominated Flows, AMD vol. 34, ASME, New York, 1979.
[22] T.R.J. Hughes, A. Brooks, A theoretical framework for Petrov-Galerkin methods with no discontinuous weighting functions: Application to the streamline upwind procedure, in: R.H. Gallagher (Ed.), Finite Elements in Fluids, vol. 4, Wiley, London, 1981.
[23] T.J.R. Hughes, L.P. Franca, G.M. Hulbert, A new finite element formulation for computational fluid dynamics. VIII. The Galerkin least squares method for advective-difussive, Comput. Methods Appl. Mech. Engrg. 73 (1989) 73–189.
[24] L. Ignat, D. Pelletier, F. Ilinca, A universal formulation of two-equation models for adaptive computation of turbulent flows, Comput. Methods Appl. Mech. Engrg. 189 (4) (2000) 1119–1139.
[25] P. Jamet, P.A. Raviart, Numerical solution of the stationary Navier–Stokes equation by finite element methods, in: R. Glowinski, J.L. Lions (Eds.), Computing Methods in Applied Sciences and Engineering, Springer, Berlin, 1973, pp. 193–223.
[26] S.W. Kim, A fine grid finite element computation of two-dimensional high Reynolds numbers flows, Comput. Fluids 16 (4) (1988) 429–444.
[27] N. Kondo, Third-order upwind finite element formulations for incompressible viscous flow problems, Comput. Methods Appl. Mech. Engrg. 93 (1991) 169–187.
[28] B. Koobus, C. Farhat, H. Tran, Computation of unsteady viscous flows around moving bodies using the k–ε turbulence model on unstructured dynamic grids, Comput. Methods Appl. Mech. Engrg. 190 (11–12) (2000) 1441–1466.
[29] O. Ladyzhenskaya, The Mathematical Theory of Viscous Incompressible Flow, Gordon & Breach, 1969.
[30] Metcalf & Eddy Inc., Ingeniería de aguas residuales, tratamiento, vertido y reutilización, McGraw-Hill, 1995.
[31] J.T. Oden, Finite Elements of Non-Linear Continua, McGraw-Hill, New York, 1972.
[32] S.V. Patankar, Numerical Heat Transfer and Fluid Flow, McGraw-Hill, 1980.
[33] B. Ramaswamy, T.C. Jue, Some recent trends and developments in finite element analysis of incompressibe thermal flow, Int. J. Numer. Meth. Engrg. 35 (1992) 671–707.
[34] J.G. Rice, R.J. Schnipke, An equal-order velocity pressure formulation that does not exhibit spurious velocity modes, Comput. Methods Appl. Mech. Engrg. 58 (1986) 135–149.
[35] P.A.B. de Sampaio, A Petrov–Galerkin formulation for the incompressible Navier–Stokes equations using equal order interpolation for velocity and pressure, Int. J. Numer. Meth. Engrg 31 (1991) 1135–1149.
[36] G.E. Schneider, G.D. Raithby, M.M. Yovanovich, Finite element solution procedures for solving the incompressible Navier–Stokes equations using equal order variable interpolation, Numer. Heat Trans. I (1978) 433–451.
[37] S.F. Shen, W. Habashi, Local linearization of the finite element methods and its application to compressible flow, Int. J. Numer. Meth. Engrg. 10 (1976) 565.
[38] T.W.H. Sheu, C.C. Fang, High resolution finite-element analysis of shallow water equations in two dimensions, Comput. Methods Appl. Mech. Engrg. 190 (20–21) (2001) 2581–2601.
[39] C. Taylor, P. Hood, A numerical solution of the Navier–Stokes equation using FEM technique, Comput. Fluids I (1973) 73–100.
[40] R. Temam, On Theory and Numerical Analysis of the Navier–Stokes Equations, North Holland, 1977.
[41] C.G. du Toit, Finite element solution of the Navier–Stokes equations for incompressible flow using a segregated algorithm, Comput. Methods Appl. Mech. Engrg. 151 (1998) 131–141.
[42] M. Turner, R. Clough, H. Martin, L. Topp, Stiffness and deflection analysis of complex structures, J. Aero Sci. 23 (9) (1956) 805–823.
[43] P. Vellando, On the resolution of the Navier–Stokes equations by the finite element method using a SUPG stabilization technique, Application to some wastewater treatment problems, Doctoral thesis, Universidad de La Coruña (Spain), Marzo, 2001.
[44] H.K. Versteeg, W. Malalasekera, An Introduction to Computational Fluid Dynamics, Harlow, UK, 1995.
[45] T. Weiyan, Shallow Water Hydrodynamics, Elsevier, 1992.
[46] O.C. Zienkiewicz, Constrained variational principles and penalty function methods in Finite Element analysis, in: G.A. Watson (Ed.), Conference of the Numerical Solution of Differential Equations, Lecture Notes in Mathematics, Springer, Berlin, 1974, pp. 207–214.

[47] O.C. Zienkiewicz, R.H. Gallagher, P. Hood, Newtonian and non-Newtonian viscous incompressible flow, temperature induced flows. Finite element solution, in: J.R. Whiteman (Ed.), The Mathematics of Finite Elements and Applications II (MAFELAP 1975), Academic Press, London, 1976.

[48] G.P.A.G. Zijl, C.G. du Toit, A simpler finite element solution of the incompressible Navier–Stokes equations. Procceedings of the Second National Symposium on Fluid Dynamics, Vereeniging, 1991, pp. 236–250.